Phosphorous doped *p*-type MoS_2 polycrystalline thin films via direct sulfurization of Mo film

Cite as: AIP Advances **8**, 025009 (2018); https://doi.org/10.1063/1.5019223
Submitted: 12 December 2017 • Accepted: 05 February 2018 • Published Online: 12 February 2018

Tomohiro Momose, Atsushi Nakamura, Moraru Daniel, et al.

Phosphorous doped *p*-type MoS_2 polycrystalline thin films via direct sulfurization of Mo film

Tomohiro Momose, Atsushi Nakamura,[a] Moraru Daniel,
and Masaru Shimomura
Graduate School of Integrated Science and Technology, Shizuoka University, 3-5-1 Johoku, Hamamatsu 432-8011, Shizuoka, Japan

(Received 12 December 2017; accepted 5 February 2018; published online 12 February 2018)

We report on the successful synthesis of a *p*-type, substitutional doping at S-site, MoS_2 thin film using Phosphorous (P) as the dopant. MoS_2 thin films were directly sulfurized for molybdenum films by chemical vapor deposition technique. Undoped MoS_2 film showed *n*-type behavior and P doped samples showed *p*-type behavior by Hall-effect measurements in a van der Pauw (vdP) configuration of 10×10 mm^2 area samples and showed ohmic behavior between the silver paste contacts. The donor and the acceptor concentration were detected to be $\sim2.6\times10^{15}$ cm^{-3} and $\sim1.0\times10^{19}$ cm^{-3}, respectively. Hall-effect mobility was 61.7 cm^{2}V^{-1}s^{-1} for undoped and varied in the range of 15.5 ~ 0.5 cm^{2}V^{-1}s^{-1} with P supply rate. However, the performance of field-effect transistors (FETs) declined by double Schottky barrier contacts where the region between Ni electrodes on the source/drain contact and the MoS_2 back-gate cannot be depleted and behaves as a 3*D* material when used in transistor geometry, resulting in poor on/off ratio. Nevertheless, the FETs exhibit hole transport and the field-effect mobility showed values as high as the Hall-effect mobility, 76 cm^{2}V^{-1}s^{-1} in undoped MoS_2 with *p*-type behavior and 43 cm^{2}V^{-1}s^{-1} for MoS_2:P. Our findings provide important insights into the doping constraints for transition metal dichalcogenides. https://doi.org/10.1063/1.5019223

Molybdenum disulfide (MoS_2), as a key material in the transition metal dichalcogenides (TMDs) family, has emerged as an attractive material and has tremendous potential for both electronic and optical applications.[1] Thus, several applications have already been reported in research, such as field-effect transistors (FETs),[2] photodetectors,[3] inverters,[4] and random access memory circuits,[5] including bio-sensors[6] and solar cells[7] due to its attractive properties such as high carrier mobility of ~100-200 cm^2/Vs at room temperature,[8] large current on/off ratio (~10^8) in FETs,[9] strong photoluminescence (PL),[10] and tunable valley spin polarization,[11] etc. For realizing these applications, both *n*- and *p*-type materials are needed to form junctions and support bipolar carrier conduction. However, particularly this point has been challenging to realize using MoS_2 due to its natural tendency for unipolar (*n*-type) transport.[12] Even though there have been various reports on *p*-type doping for MoS_2, such as nitrogen plasma-assisted doping on exfoliated MoS_2,[13–15] phosphorous ion implantation,[12] a substitutional doping using niobium (Nb) in bulk MoS_2,[16,17] respectively, such efforts are limited to nano- or micro-scale flakes of MoS_2 obtained from bulk materials. Therefore considerable efforts are required for scalable synthesis of *p*-type MoS_2 film to realize practical applications. To date, a direct growth method of MoS_2 thin films by chemical vapor deposition (CVD) via vapor-phase reaction of MoO_3 and sulfur (S) powders,[18–21] $MoCl_5$ and S powders,[22,23] and metal Mo films[24–28] in a CVD furnace have been demonstrated to overcome a large area film synthesis. Among them, the direct grown method of TMDs (e.g. MoS_2) synthesis via sulfurization of transition metal films has great

[a]Corresponding author: nakamura.atsushi@shizuoka.ac.jp

advantages for a large scale to have possibilities for the band gap engineering,[29] hetero-structures,[30] and doping.[25] Laskar *et al.*[25] first reported on *in situ p*-type doping in cation-site by Nb diffusion in direct grown MoS_2 thin films. However, there are only a few reports for *in situ p*-type doping in anion-site using an acceptor dopant in film growth of MoS_2.[31] Foreign element doping is an important strategy to realize electric applications, and especially for the MoS_2 has a natural tendency of *n*-type behavior owing to S-vacancy, an anion-site substitution technique is thought to be effective on realizing stable *p*-type MoS_2.

In this study, we provide a first experimental report on an anion substitutional doping on MoS_2 by phosphorous. MoS_2 films were synthesized via Mo thin film sulfurization on SiO_2/Si. According to previous literature,[32,33] in a doping strategy, group V elements of nitrogen (N_2), phosphorous (P), arsenic (As) are candidates for an acceptor in MoS_2. Among these elements, P is a suitable acceptor because it is a stable solid-state material in air, is compatible with semiconductor dopant, and is a harmless material. We examine film growth of thermal sulfurization of molybdenum with different phosphorus flow contents. The films were characterized by Raman spectroscopy of the crystal structure, reflectance and photoluminescence spectra for the bandgap of MoS_2 film and electrical evaluations by Hall-effect measurements. We also demonstrate the transport property of field-effect transistors comparing with undoped MoS_2 film and confirmed that phosphorus acts as a *p*-type dopant in MoS_2.

We performed direct growth of MoS_2 thin film on SiO_2/Si substrates by the vapor-phase reaction of metal Mo film and S powders in a hot-wall CVD system. The schematic illustration of the experimental set-up was presented in S1 of the supplementary material. The quartz tube reactor was pumped down using a rotary pump with a pressure controller, and placed inside a furnace. The substrates were placed in the center of an electric furnace with a quartz tube reactor. Commercially available SiO_2 (95nm)/*p*-Si (100) wafer was used as a substrate after washing with acetone, ethanol, H_2SO_4/H_2O_2, and ultrapure water. Before sulfurization, around 1.3 nm thick Mo films were deposited by a resistance heating type vacuum evaporator using Mo wire (radius of 0.2 mm) itself as a Mo source on SiO_2/Si substrates. High purity sulfur powder (99.99%) and phosphorus powder (99.99%) were placed in each different ampoules made by Al_2O_3 crucible with a quartz glass cover to maintain the vapor pressure of sulfur and phosphorus and were placed in a hot second and third upstream zone. Next, the substrates with Mo film deposited were placed in a quartz tube furnace and heated at 850°C for 60 min with a heating rate of 20°C/min and Ar flow (200 sccm) at the pressure of 100 Torr. The temperature evolution of the reaction furnace and the heating belt for sulfur and phosphorus evaporation is shown in S2 of the supplementary material. Prior to sulfurization of Mo film, the Mo film was treated with hydrogen: argon = 20: 180 sccm flow at the growth temperature for 15 min to remove oxide impurity. The flow rate of S and P vapor were calculated from the ratio of partial pressure of each vapor pressure controlled by the heater temperature. The relationship between the heater temperature and the flow rate is shown in Fig. S3 of the supplementary material and the experimental condition were summarized in Table SI of the supplementary material. The film thickness of MoS_2 layer has been studied by means of measure AFM height difference between the total film height and the substrate surface. Fig. S4 of the supplementary material shows typical AFM images of the Mo, MoS_2, and MoS_2:P samples. The film thickness in this experiment was controlled at 5 nm.

The samples were prepared in two geometries. One was with the film homogeneously grown over the whole substrate for Hall-effect measurement to employ four contacts on four corner of the substrate in van der Pauw configuration. The contact electrodes were deposited silver (Ag) paste. The other was for fabricating back-gate type FETs, and for deposition of contacting metal leads a metal shadow mask was aligned with the pre-structured MoS_2. Ni films (100nm) were deposited by using an electron beam evaporation system. The two types of samples were simultaneously grown in the reactor to make same growth condition.

The thickness and surface morphology were measured using atomic force microscope (AFM, VN-8000, KEYENCE). Raman spectra and photoluminescence (PL) spectra were obtained by Raman microscopic systems (NRS-7100, JASCO Inc.) with wavelength and spot size of the laser of 532 nm and 0.1 μm, respectively. The Si peak at 520.4 cm^{-1} was used for calibration in the experiments. Room temperature photoluminescence (PL) was utilized for characterizing the optical quality of the MoS_2 film. Reflectance spectra were obtained by UV-VIS-NIR optical scanning spectrometer (UV-3100PC,

SHIMAZU). The electrical measurements were performed at room temperature by using a Keithley 4200-SCS Semiconductor Characterization System connected to a probe station.

As shown in Figure 1(a), it was found that the two typical Raman active modes could be obtained from the frequencies of E^1_{2g} and A_{1g} peaks in all samples. The E^1_{2g} peak and the A_{1g} peak in the undoped MoS_2 film are located at 379.3 cm^{-1} and 405.3 cm^{-1}, giving a frequency difference of ~26.0 cm^{-1}.[34] It indicated that the synthesized 5 nm thick MoS_2 films are compatible with the bulk MoS_2 layer. When we increased phosphorus dose for 41 μmol/min, the E^1_{2g} peak corresponding to an in-plane vibrational mode slightly blue-shifted. The blue shift of the E^1_{2g} mode with respect to the undoped MoS_2 suggests that the type of strain generated due to the presence of Mo–P bonding is compressive.[14] Azcatl *et al.*[14] first reported that strain induced by a single atom dopant in MoS_2 treated with a remote plasma N_2 exposure could be verified by observing its Raman spectrum, and they have confirmed that the presence of nitrogen can induce compressive strain in the MoS_2 structure. The calculated Mo-S bond length is 2.411 Å, the Mo-P bond length of 2.410 Å is slightly shorter than that of Mo-S,[31] which suggests a contraction of the MoS_2 lattice due to the introduction of phosphorus as a dopant. For the 172 μmol/min doped sample, the A_{1g} peak blue-shifted by 0.1 cm^{-1}, which is also a compressive strain effect, reflected as a shift of the out-of-plane vibrational mode A_{1g}. This hypothesis is attributed to a subsequent formation of P-Mo-P in co-doping nature is partially possible in the comparatively high P dose condition (the flow ratio of S: P = 187: 172 μmol/min, P/S = 92.0 %), a compressive strain generated due to the shorter distance of P-P (2.876 Å) than that of S-S (3.141 Å) in pure MoS_2 system.[31]

Optical transitions in undoped MoS_2 film and MoS_2: P sample were identified using reflection spectroscopy. Reflectivity differences between the bare SiO_2/Si substrate and regions of the MoS_2 film were measured across the visible and near IR spectral range (Fig. 1(b)). Two prominent absorption peaks can be identified as 1.82 eV and 1.99 eV in the spectrum. These two peaks can be assigned to be the direct excitonic transitions at the Brillouin zone *K* point, and the two resonances are known as *A* and *B* excitons, respectively.[35] Optical absorption of the indirect bandgap (~1.2 eV) is supposed to be very weak. PL spectra of undoped MoS_2 film on the bottom and MoS_2:P sample on top were displaced along the vertical axis of the differential reflectance to be specified. In undoped MoS_2, pronounced luminescence emissions were observed at the *A* direct excitonic transitions and indirect transitions (*I*). The *A* peak in PL is almost equivalent in energy in optical absorption of *A* excitons in the differential

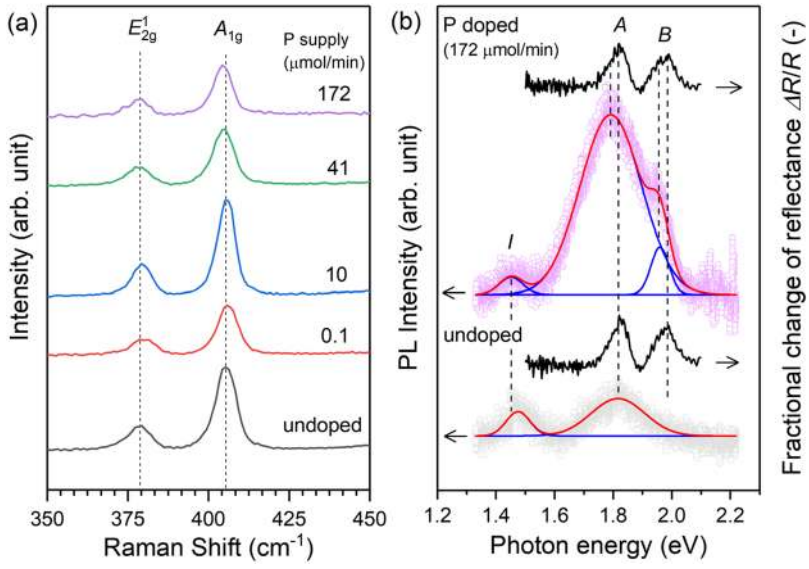

FIG. 1. (a) Raman spectra of undoped MoS_2 film and phosphorus doped MoS_2 samples for supply flow rate 0.1, 10, 41, and 172 μmol/min, respectively. The left and right dashed lines show the positions of the E^1_{2g} and A_{1g} peaks in MoS_2, respectively. (b) PL spectra of undoped MoS_2 and MoS_2:P samples and differential reflectance spectra. The PL and reflectance spectra were recorded at room temperature.

reflectance spectra. Indirect emission yields low compared with the *A* direct recombination owing to the emission process having with electron-hole pairs separated in the *K*-space. In MoS_2:P sample, emission peaks *A* and *B* match the two absorption resonance with a slightly red-shift. The red-shifts are attributed to the Stokes shifts, and the magnitude of the Stokes shift is reported to increase with doping level.[36]

I-V properties, resistivity, carrier concentration, and Hall-mobility of the undoped MoS_2 and MoS_2:P samples were measured using a Hall-effect measurement system via the four measured points on the samples at the dark condition, as showed in Fig. 2. The currents of the samples display a linear dependence on the applied voltage, indicating that the contacts between the film and Ag paste have an ohmic behavior. Compared with the slopes of the *I-V* curves of undoped MoS_2, the MoS_2:P sample has a large slope and a significant reduction in resistivity when P ions are doped at higher P-supply rates. A typical resistivity of undoped MoS_2 is 99.4 Ωcm. The resistivity value for the MoS_2:P is gradually decreased with doping level as showed in Fig. 2(b). Transport behavior of undoped MoS_2 shows *n*-type conductivity and that of MoS_2:P samples show *p*-type conductivity. The carrier concentrations are gradually increased with P supply flow rate, -2.5×10^{15} cm^{-3} for undoped MoS_2 and $+1.0\times10^{19}$ cm^{-3} for higher doped MoS_2:P (Fig. 2(c)). Finally, the Hall-mobility in undoped MoS_2 is calculated to be 61.7 $cm^2V^{-1}s^{-1}$ and the mobility in MoS_2:P was gradually decreased from 15.5 $cm^2V^{-1}s^{-1}$ to 0.5 $cm^2V^{-1}s^{-1}$ with P doping levels (Fig. 2(d)).

The impact of phosphorus doping on transport properties was evaluated by fabricating transistors comparing with the undoped MoS_2 sample. Electrical measurements were performed to characterize the electrical conductivity of the device at room temperature. Figure 3(a) displays the I_{DS} versus V_{DS} curves of undoped MoS_2. Interestingly, undoped MoS_2 exhibits double Schottky *I-V* behavior and showed *p*-type conduction with a poor I_{ON}/I_{OFF} ratio ($\sim10^0$) (Fig. 3(b)), though it exhibits *n*-type conductivity in Hall-effect measurements. The insets of Fig. 3(a) illustrate a cross-section schematic of the device and the possible image of an energy band diagram of MoS_2 and Ni source/drain contacts. The transfer characteristics of I_{DS}-V_G curves for undoped MoS_2 were extracted for different values

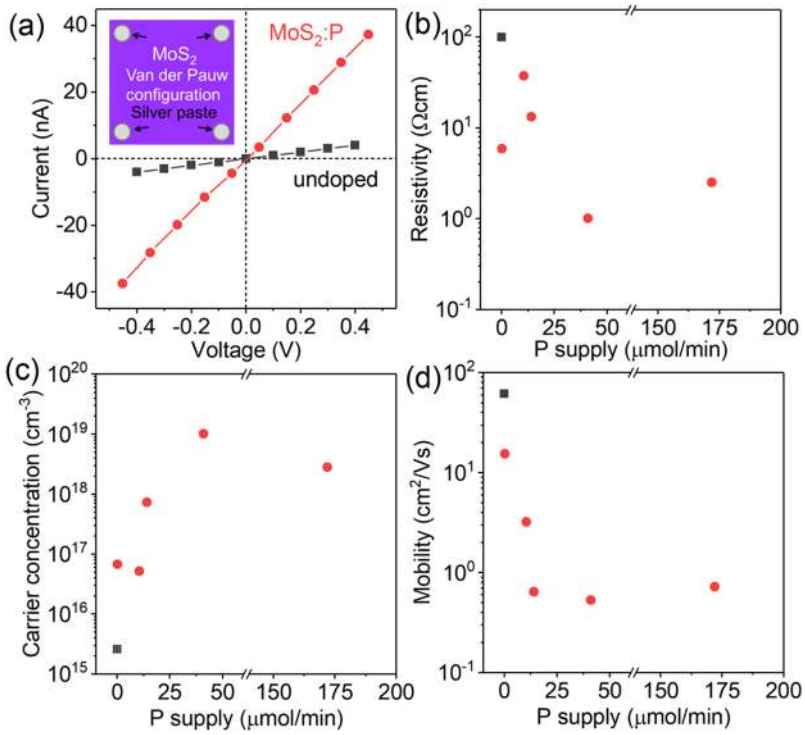

FIG. 2. (a) *I-V* characteristics of the undoped MoS_2 film and the MoS_2:P film. The inset shows in the drawing of a sample configuration of van der Pauw with Ag paste electrodes. Results of Hall-effect measurements in the dark condition for (b) Resistivity, (c) Carrier concentration, and (d) Hall mobility, respectively.

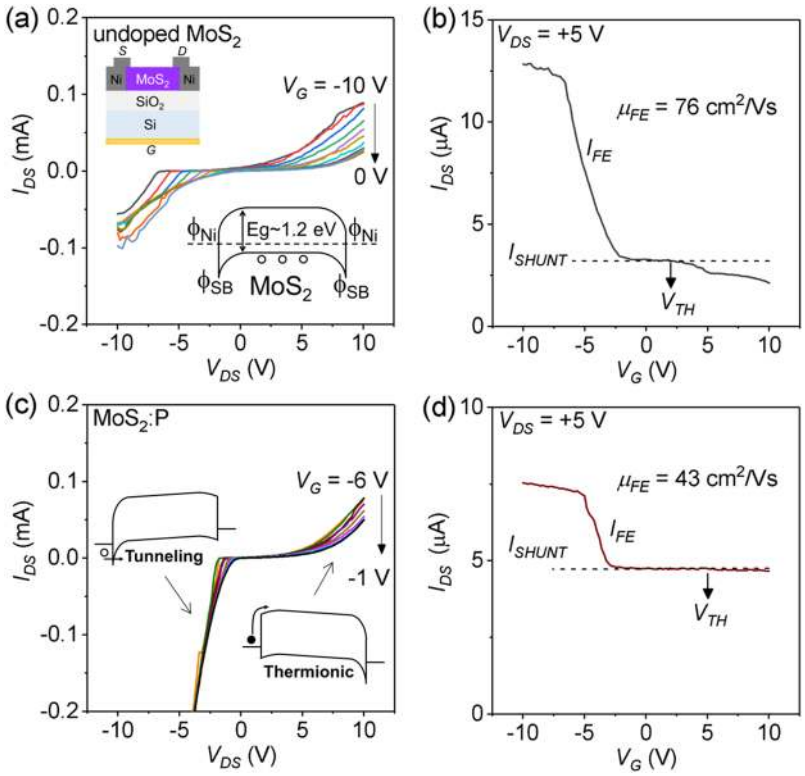

FIG. 3. Characterization of back-gated FETs with Ni contact. The FET device was measured a T=300 K (room temperature). Device geometry is: W/L = 0.5/300 mm, t_{ax} = 95 nm and t_{ch} = 20 nm. (a) Drain current versus drain bias (I_{DS}-V_{DS}) curve for the undoped MoS_2 device. The back-gate bias (V_G) varies 0 V to -10 V with a 1 V step. The inset in the upper left shows a schematic device structure of a back-gated FET on 95 nm SiO_2 substrate with Ni. The inset at the lower right shows the band diagram of a double Schottky barrier between Ni source/drain and MoS_2. (b) Transfer characteristics of I_{DS}-V_G curve for the sample (a), V_{DS} = +5 V. (c) I_{DS}-V_{DS} curves of MoS_2:P sample. V_G varies -6 V to -1 V with a 0.5 V steps. The insets show in the band diagram according to the reverse and forward bias conditions. (d) I_{DS}-V_G curves for the sample (c), V_{DS} = +5 V.

of V_G with a constant drain-source voltage at 5 V (Fig. 3(b)). As it is clear from the plot, the p-type behavior of the device with negative back-gate voltage results in higher drain current. In other words, a reduction in current along with a positive threshold voltage (V_T) shift to higher gate voltage is observed. Furthermore, it shows the different components of the source to drain current such as I_{FE} and I_{SHUNT} in the 5 nm thick undoped MoS_2 film. The I_{FE} is the current associated with the depletion layer and follows the conventional gate voltage dependence given by the following equation:[17]

$$I_{FE} = \mu_p \left(\frac{W}{L}\right) V_{DS} C_{OX} \left(V_G - V_T\right), \tag{1}$$

$$I_{SHUNT} = \mu_p \left(\frac{W}{L}\right) V_{DS} q N_A \left(t_{body} - W_{DM}\right), \tag{2}$$

where μ_p is the hole mobility, W and L are the channel length (W: 0.5 mm, L: 3 mm), and C_{OX} is the oxide capacitance. $C_{OX} = \varepsilon_{OX}/d_{OX}$, where ε_{OX} is the dielectric constant and d_{OX} is the thickness of the gate oxide, d_{OX} = 95 nm and for SiO_2, ε_{OX} = 3.6×10^{-11} F/m, which gives C_{OX} ~3.6×10^{-4} F/m^2. Elemental charge q = 1.6×10^{-19} C, N_A is an extrinsic doping concentration, t_{body} is the thickness of MoS_2 channel, W_{DM} is a maximum width of depletion, respectively. The field effect mobility of undoped MoS_2 is estimated using $\mu = [dI_{DS}/dV_G] \times [(L/(WC_{OX}V_{DS})]$. The field-effect mobility of undoped MoS_2 was found to be 76 cm^2/Vs. However, in our MoS_2 FET, the thickness of the semiconducting channel is extremely more than the maximum width of the depletion region, and the device cannot be depleted, thus a shunting path for the current is dominant,

and the device cannot be turned OFF. Figure 3(c) shows I_{DS}-V_{DS} curves of MoS_2:P sample. *I-V* curves showed highly rectifying behavior in contrast to the undoped MoS_2 device (Fig. 3(a)). Insets represent energy band diagrams corresponding to the applied drain biases in the negative ($V_{DS} < 0$ V) and the positive ($V_{DS} > 0$ V) biasing regions. Although this sample was expected to be *p*-type conduction, significant *p*-type transport was not observed since the contacts are strongly pinned near the conduction band. As a speculation from the *I-V* curves with negative V_{DS} region, holes are injected from the source electrode, and then a tunneling current was observed. In positive V_{DS} region, electrons from the source electrode were retained for the energy barrier, a thermionic current was observed. Figure 3(d) shows transfer characteristics of a back-gated MoS_2:P transistor. We observed a reduction in current along with a positive threshold voltage (V_T) shift toward higher gate voltage after *p*-type doping. Furthermore, a magnitude of the shunt current was larger as 4.7 μA compared with undoped one (3.2 μA), suggesting doped acceptor level (N_A) was increased. The result is agreed with a reduction of the resistivity in *I-V* characteristics as showed in Fig. 2(a). Calculated mobility was 43 cm^2/Vs.

Here, we discuss the reason why the carrier conductivity type was observed conflicting. Currently, there is argument on the conductivity of undoped MoS_2. The majority of recent studies of undoped MoS_2 conductivity report *n*-type behavior,[2,8,9,12–14,37–40] and the previous studies revealed that the Fermi-level tends to be pinned at charge neutrality level or sulfur vacancy level which is located below the conduction band edge, so electrons are injected, thus making MoS_2 conductivity mostly *n*-type.[37] Furthermore, MoS_2 transistors are essentially Schottky barrier transistors, and thus the charge injection from the source electrode degrades the transistor output. On the other hand, *p*-type behavior of undoped MoS_2 is also reported.[27,41,42] Most important things that they have measured the devices under vacuum conditions. McDonnell, *et al.*[43] pointed out that MoS_2 can exhibit both *n*-type and *p*-type conduction, where are related to intrinsic defects. In our device, the undoped MoS_2 was probably *p*-type in 5 nm thickness (~7, 8 layers), but the surface top layer was *n*-type doped by intrinsic defects such as sulfur vacancy and chemo-absorbed molecules. Note that the device geometry and contact-electrodes on MoS_2 in this experiment are different between the samples in Hall-effect measurements via van der Pauw geometry and the field effect transistors. Figure 4 shows schematic cross-sectional illustrations of each device structure and shows a possible current path through the devices. For the vdP samples, the electrodes are formed on the MoS_2 surface. The surface exhibits 2*D* crystal nature and is regarded as less absence of dangling bonds. Besides, the MoS_2 film is fully covered on the substrate, and there is no edge of the body at the current path along with the four electrodes. The metal contact lies on top of the MoS_2 layers, then the current path may be limited by tunneling through the van der Waals gap, the surface exhibits intrinsic defects such as sulfur vacancy and ambient interactions such as physical or chemical absorption[12] result in strong *n*-type behavior can be detected in MoS_2 vdP measurements. Besides, the metallic character of sulfur vacancies can effectively lower Schottky barrier height[40] resulting in ohmic behavior in

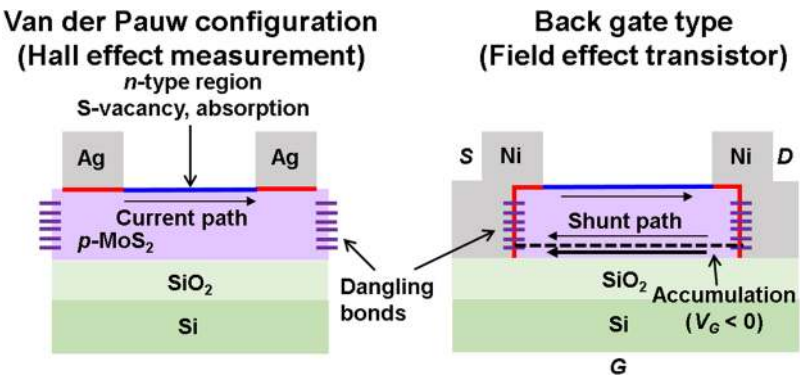

FIG. 4. Schematic cross-sectional illustrations of each device structure and shows a possible current path through the devices. The blue line indicates the *n*-type region for the surface of MoS_2 layer. The red line highlights the contact interface between the metals and MoS_2.

the *I-V* characteristics as shown in Fig. 2(a). In contrast, FET channels were made to the strip-bar structure. The source/drain electrodes covered MoS_2 surface and cross-sectional walls similarly to three-dimensional semiconductors. The density of the interface states is considerably high because of the electronic states arising from surface dangling bonds, resulting in a large Schottky barrier.[39] The drain current can be divided into two components as I_{FE} and I_{SHUNT}. Furthermore, the I_{SHUNT} includes electrons running through the surface *n*-type layer even the main body of undoped MoS_2 tends to *p*-type conductivity. Therefore, a precise determination of *p*-type doping profiles via characterization of FET was more complicated in this work, and it is possible that the *p*-type behavior of P-doped MoS_2 comes from MoS_2 itself partly.

In conclusion, we have demonstrated *p*-type doping of MoS_2 using a phosphorus as the dopant. MoS_2 thin films were directly sulfurized for molybdenum films by chemical vapor deposition technique. Impacts of phosphorus doping were characterized by optical analysis and electrical transport properties. We show that P can act as an efficient acceptor in MoS_2 with relatively high mobility. For a hole concentration of 1×10^{19} cm^{-3}, Hall-mobility of 0.53 cm^2/Vs and a field-effect mobility of 43 cm^2/Vs were achieved. Although there are still remaining an obstacle issues for contact problems as Schottky behavior, the use of P substitutional impurity for *p*-type doping demonstrated in this work for MoS_2 could be extended to other dichalcogenides such as TM-(S, Se) systems.

SUPPLEMENTARY MATERIAL

See supplementary material for the experimental details and thickness evaluations of MoS_2 films.

ACKNOWLEDGMENTS

This work was supported by Japan Society for the Promotion of Science (JSPS), JSPS KAKENHI, Grant-in-Aid for Young Scientists (B) JP26870247, and Grant-in-Aid for Scientific Research (B) JP17H03402 and a part of this research is based on the Cooperative Research Project of Research Center for Biomedical Engineering, Ministry of Education, Culture, Sports, Science, and Technology.

[1] A. H. Castro Neto and K. Novoselov, Rep. Prog. Phys. **74**, 082501 (2011).
[2] S. Bhattacharjee, K. L. Ganapathi, S. Mohan, and N. Bhat, Appl. Phys. Lett. **111**, 163501 (2017).
[3] S. Luo, X. Qi, L. Ren, G. Hao, Y. Fan, Y. Liu, W. Han, C. Zang, J. Li, and J. Zhong, J. Appl. Phys. **116**, 164304 (2014).
[4] X. He, W. Chow, F. Liu, B. Tay, and Z. Liu, Small **13**, 1602558 (2017).
[5] H. Wang, L. Yu, Y. Lee, Y. Shi, A. Hsu, M. L. Chin, L. Li, M. Dubey, J. Kong, and T. Palacios, Nano Lett. **12**, 4674 (2012).
[6] D. Sarkar, W. Liu, X. Xie, A. C. Anselmo, S. Mitragotri, and K. Banerjee, ACS Nano **8**, 3992 (2014).
[7] S. Lin, X. Li, P. Wang, Z. Xu, S. Zhang, H. Zhong, Z. Wu, W. Xu, and H. Chen, Sci. Rep. **5**, 15103 (2015).
[8] S. Kim, A. Konar, W.-S. Hwang, J. Lee, J. Lee, J. Yang, C. Jung, H. Kim, J.-B. Yoo, J.-Y. Choi, Y. Jin, S. Lee, D. Jena, W. Choi, and K. Kim, Nat. Commun. **3**, 1011 (2012).
[9] W. Wu, D. De, S.-C. Chang, Y. Wang, H. Peng, J. Bao, and S.-S. Pei, Appl. Phys. Lett. **102**, 142106 (2013).
[10] Y. Zhu, J. Yang, S. Zhang, S. Mokhtar, J. Pei, X. Wang, and Y. Lu, Nanotech. **27**, 135706 (2016).
[11] K. Mak, K. He, J. Shan, and T. F. Heinz, Nat. Nanotech. **7**, 494 (2012).
[12] A. Nipane, D. Karmakar, N. Kaushik, S. Karande, and S. Lodha, ACS Nano **10**, 2128 (2016).
[13] M. Chen, H. Nam, S. Wi, L. Ji, X. Ren, L. Bian, S. Lu, and X. Liang, Appl. Phys. Lett. **103**, 142110 (2013).
[14] A. Azcatl, X. Qin, A. Prakash, C. Zhang, L. Cheng, Q. Wang, N. Lu, M. J. Kim, J. Kim, K. Cho, R. Addou, C. L. Hinkle, J. Appenzeller, and R. M. Wallace, Nano Lett. **16**, 5437 (2016).
[15] P. Mishra, M. Tangi, T. Ng, M. Hedhili, D. Anjum, M. Alias, C.-C. Tseng, L.-J. Li, and B. Ooi, Appl. Phys. Lett. **110**, 012101 (2017).
[16] R. S. Title and M. W. Shafer, Phys. Rev. Lett. **28**, 808 (1972).
[17] S. Das, M. Demarteau, and A. Roelofs, Appl. Phys. Lett. **106**, 173506 (2015).
[18] M. R. Laskar, D. N. Nath, L. Ma, E. W. Lee, C. Lee, T. Kent, Z. Yang, R. Mishra, M. A. Roldan, J.-C. Idrobo, S. T. Pantelides, S. J. Pennycook, R. C. Myers, Y. Wu, and S. Rajan, Appl. Phys. Lett. **104**, 092104 (2014).
[19] H. Ago, H. Endo, P. Solís-Fernández, R. Takizawa, Y. Ohta, Y. Fujita, K. Yamamoto, and M. Tsuji, ACS Appl. Mater. Interface. **7**, 5265 (2015).
[20] J. D. Cain, F. Shi, J. Wu, and V. P. Dravid, ACS Nano **10**, 5440 (2016).
[21] D. Kaplan, K. Mills, J. Lee, S. Torrel, and V. Swaminathan, J. Appl. Phys. **119**, 214301 (2016).
[22] A. Rajan, J. H. Warner, D. Blankschtein, and M. S. Strano, ACS Nano **10**, 4330 (2016).
[23] K. McCreary, A. Hanbicki, J. Robinson, E. Cobas, J. Culbertson, A. Friedman, G. G. Jernigan, and B. T. Jonker, Adv. Funct. Mater. **24**, 6449 (2014).
[24] L. Samad, S. Bladow, Q. Ding, J. Zhuo, R. Jacobberger, M. Arnold, and S. Jin, ACS Nano **10**, 7039 (2016).
[25] Y. J. Zhang, J. T. Ye, Y. Yomogida, T. Takenobu, and Y. Iwasa, Nano Lett. **13**, 3023 (2013).

[26] C. M. Orofeo, S. Suzuki, Y. Sekine, and H. Hibino, Appl. Phys. Lett. **105**, 083112 (2014).
[27] Y. Zhan, Z. Liu, S. Najmaei, P. M. Ajayan, and J. Lou, Small **8**, 966 (2012).
[28] Y. Lim, Y. Lee, S. Kim, S. Kim, Y. Kim, C. Jeon, W. Song, S. Myung, S. S. Lee, K.-S. An, and J. Lim, Appl. Surf. Sci. **392**, 557 (2017).
[29] Y. Xue, Y. Zhang, Y. Liu, H. Liu, J. Song, J. Sophia, J. Liu, Z. Xu, Q. Xu, Z. Wang, J. Zheng, Y. Liu, S. Li, and Q. Bao, ACS Nano **10**, 573 (2016).
[30] Y. Gong, Z. Liu, A. Lupini, G. Shi, J. Lin, S. Najmaei, Z. Lin, A. Elías, A. Berkdemir, G. You, H. Terrones, M. Terrones, R. Vajtai, S. Pantelides, S. Pennycook, J. Lou, W. Zhou, and P. Ajayan, Nano Lett. **14**, 442 (2014).
[31] G. Wang, H. Yuan, A. Kuang, and H. Chen, Phys Stat. Sol. B1700413 (2017).
[32] K. Dolui, I. Rungger, C. Pemmaraju, and S. Sanvito, Phys. Rev. B **88**, 075420 (2013).
[33] L. Zhang, T. Liu, T. Li, and S. Hussain, Physica E **94**, 47 (2017).
[34] S. Wang, X. Wang, and J. Warner, ACS Nano **9**, 5246 (2015).
[35] A. Splendiani, L. Sun, Y. Zhang, T. Li, J. Kim, C.-Y. Chim, G. Galli, and F. Wang, Nano Lett. **10**, 1271 (2010).
[36] K.-I. Lin, Y.-J. Chen, B.-Y. Wang, Y.-C. Cheng, and C.-H. Chen, J. Appl. Phys. **119**, 115703 (2016).
[37] H. Liu, M. Si, Y. Deng, A. Neal, Y. Du, S. Najmaei, P. Ajayan, J. Lou, and P. Ye, ACS Nano **8**, 1031 (2014).
[38] J. Suh, T. E. Park, D. Y. Lin, D. Fu, J. Park, H. J. Jung, Y. Chen, C. Ko, C. Jang, Y. Sun, R. Sinclair, J. Xhang, S. Tongay, and J. Wu, Nano Lett. **14**, 6974 (2014).
[39] R. Nouchi, J. Appl. Phys. **120**, 064503 (2016).
[40] J. Su, L. Feng, Y. Zhang, and Z. Liu, Nanotechnology **28**, 105204 (2017).
[41] Z. Zeng, Z. Yin, Z. Huang, H. Li, Q. He, G. Lu, F. Boey, and H. Zhang, Angew. Chem. Int. Ed. **50**, 11093 (2011).
[42] M. Meng and X. Ma, Nanoscale Res. Lett. **11**, 513 (2016).
[43] S. McDonnell, R. Addou, C. Buie, R. M. Wallace, and C. L. Hinkle, ACS Nano **8**, 2880 (2014).